*Mediterranean Archaeology and Archaeometry*
*Vol. 19, No 2, (2019), pp. 81-104*
*Open Access. Online & Print.*

*www.maajournal.com*

**DOI: 10.5281/zenodo.3239053**

# DIGITAL MACRO-PHOTOGRAMMETRY IN DOCUMENTATION OF OLD TURKIC RUNIFORM INSCRIPTIONS IN THE ALTAI MOUNTAINS

**Mikhail Vavulin[1], Irina Nevskaya*[1 2 3] and Larisa Tybykova[4]**

*[1]Laboratory of linguistic anthropology, Tomsk State University, Tomsk, Russia*
*[2]Departament of Comparative Linguistics, Phonetics and Slavonic Studies, Frankfurt University, Frankfurt, Germany*
*[3]Institute of Philology Siberian Branch of the Russian Academy of Sciences, Novosibirsk, Russia*
*[4]Gorno-Altaisk State University, Gorno-Altaisk, Russia*

**Received: 15/05/2019**
**Accepted: 03/06/2019**
**Corresponding author: I. Nevskaya (nevskaya@em.uni-frankfurt.de)*

## ABSTRACT

The article presents a method of the 3D digitization of rock surfaces ensuring a sub-millimeter resolution. The method was developed for documenting Old Turkic inscriptions of the Altai Mountains mostly made by fine engravings on rock outcrops. These are the earliest sources on the history, language and culture of ancient Turkic peoples written in an autochthonous runiform script. The method involves the digital photogrammetry technology "Structure from Motion" (SfM) based on a set of macro photos. It was tested in the laboratory and in the field conditions, the accuracy and deviations of the obtained 3D models of documented planes were determined. The data of the obtained 3D models were extracted in the bitmap format (as height maps and orthophotos), and analyzed in the GIS application. The method was applied for documenting recently discovered and not yet published Altai runiform inscriptions in the localities D'odro and Karban; it helped to distinguish the lines of the inscriptions from those of numerous graffiti and other lines, and to decipher them. The article presents the first publication of the inscriptions D'odro I and Karban IV, including the copies based on the 3D models along with their readings, interpretations and translations.

**KEYWORDS:** 3D, macrophotography, digital photogrammetry, SfM, ancient Turks, autochthonous runiform script, Altai Mountains, runiform inscriptions D'odro I and Karban IV.

## 1. INTRODUCTION

Old Turkic runic inscriptions (or, better, runiform ones, as they are not genetically connected with Old Germanic runes; both terms are used further as synonyms) are the earliest Turkic sources approximately dating back to the 6th - 12th centuries AD and providing valuable information on the history, culture and language of ancient Turkic peoples. These inscriptions are scattered all over Eurasia; they constitute a corpus of several hundreds of inscriptions. Written in an autochthonous script on rocks, steles and everyday objects, they present a great challenge for researchers trying to decipher them. The most famous and studied ones are the so called Orkhon inscriptions in Mongolia, followed by runic epitaphs in the reaches of the river Yenisei in the Republics of Tyva and Khakassia (Russian Federation), and in the Talas and Kochkor valleys in the Republic of Kyrgyzstan.


*Figure 1. Republic of Altai. Work points 2018.*

The Old Turkic runic inscriptions in the Republic Altai (Fig. 1) are special in many ways, and very difficult for reading. Extremely fine engravings on rock outcrops make them hardly seen even at a close distance. They are rarely epitaphs following the classical canons of the Orkhon and Yenisei inscriptions, but often philosophical, religious or very personal texts, written by the ancient Turkic population at large. Moreover, they are written in a non-canonical orthography as compared to the orthography of the "classical" Orkhon inscriptions and employ some runiform signs not found in the latter. All this hampered research on them for a long time. Only in the course of the recent decades, they have become an object of special research (e.g. Tybykova et al., 2012).

Beside the specific linguistic problems, there is a problem of an adequate documentation of the writing itself. There are many variations of reading of the same inscription because of its improper copying (cf. Konkobaev et al., 2015; Tybykova et al., 2012). The

inscriptions are made on rock surfaces with the area ranging from 0.02 to 1.0 m². They vary widely in length and may consist of several characters, or of several lines. The characters themselves are fine cuts of 0.1 – 1.0 mm width. Their depth is sometimes less than 0.1 mm. The height of the characters is typically from 1 to 3 cm. Such size creates serious difficulties in documenting the runic signs and their subsequent interpretation. The originally well-seen characters have blended in with the rock surface color under the effect of the aggressive natural environment. Some cuts can hardly be distinguished from the natural fractures and erosion of the rock because they are small in size and not cut deeply enough into the rock surface. Sometimes it is difficult to distinguish the lines belonging to the runic inscription because of the acts of vandalism of tourists who make their own graffiti over the ancient inscriptions. In addition, the used rock surfaces had been palimpsests already in the ancient times because they had been used for graffiti and petroglyphs for centuries. In view of these circumstances, we have to fulfill the task of a detailed digitization of the rock surfaces with runic inscriptions first, in order to distinguish the lines of the runic characters from other lines on the surface and to interpret the inscriptions. For this purpose, it is important both to make a 3D fixation of the surface for the subsequent texture analysis, and to ensure an adequate color fixation.

## 2. POSSIBLE SOLUTIONS

The Reflectance Transformation Imaging (Polynomial texture mapping) technology is widely used in the sphere of studying and preservation of the cultural heritage (Mudge et al., 2005). This technology is based on processing of multiple object images with fixed positions of the object and the camera but with varying position of the light source. The RTI technology is a perfect means for the surface texture visualization. It has proven itself in the work on petroglyphs (e.g. Cassen et al., 2015; Díaz-Guardamino et al., 2015; Mudge et al., 2006) and inscriptions (Vovin, 2018; Maue, 2018). However, because of the above-mentioned features of the Altai inscriptions, we have chosen an approach based on the full-scale 3D fixation of the surface.

Multiple projects with 3D digitization of rock surfaces have been implemented recently (e.g. Alexander et al., 2015; Bea and Angás, 2017; Cassen et al., 2014; Robert et al., 2016; Zeppelzauer et al., 2016). Digitization of artefacts made of stone has also been done with the purpose of tracing the engravings on surfaces (e.g. Porter et al., 2016). However, all these works were aimed at either a high resolution shooting of small surface areas, or at an overall surface recording with lower resolution.

The following solutions can be applied for a 3D digitization of rock surfaces with high resolution.

The most convenient solution ensuring high mobility involves the use of portable 3D scanners. There are several models of manual 3D scanners on the market today, allowing for objects' digitization with resolution from 0.1 to 0.05 mm. However, all these options are expensive, and, in many cases, the possible resolution would not be sufficient. Using less expensive 3D structured light scanners (SLS), which may ensure scanning with sufficiently high resolution, seems to be the optimal solution (Maté-González et al., 2017). Although these scanners are intended for stationary operation conditions, their size allows for their transportation and use in the field. The SLS scanners ensure quite high resolution in the minimal scanning area – even the relatively inexpensive models may provide resolution up to 0.03 mm. However, for digitizing the whole rock surfaces, the problem of a correct alignment of a variety of individual 3D frames into the single surface arises. In addition, the structured light scanners are highly dependent on the ambient light and require an external power supply. It is quite difficult to ensure functioning of this equipment in case a runic inscription is located in a hard-to-reach place in the mountains.

Moreover, not all SLS scanners support texture capturing and laying the texture over the obtained 3D model. In some cases, an analysis of colors may play the key role for distinguishing the lines of petroglyphs and inscriptions on the same rock. Use of the D-stretch program for finding distortions of the color information in an image has given good results for studying petroglyphs (Fernández-Lozano et al., 2017; Jalandoni et al., 2018; Rogerio-Candelera, 2015). In some cases, this method can be used for recognition of runic characters as well.

Along with scanning, some 3D models' generation technologies using photos, e.g. building a model from a series of frames with various focuses «Shape from focus» (Subbarao and Choi, 1995), or digital photogrammetry «Structure from motion», can be used for digitizing objects with high resolution. The first of these technologies is applicable for documenting micro-traces on a small area because it is only capable of generating a 3D model of an area that fits within one frame. It is reasonable to use this technology when working with the camera's manifold zooming, especially for traceology (Plisson, 2015). However, the necessity of generation of the full-scale 3D polygon nets of a rock surface containing both runic inscriptions and petroglyphs makes the use of the "shape from focus" technology impossible for the purpose.

The digital photogrammetry is widely used in archaeology (Tsiafaki and Michailidou, 2015; Howland et al. 2014) and The digital photogrammetry technology allows generating 3D models of the objects using their close-up photos taken under various angles (Kovalev et al., 2017; Maté González et al., 2015; Plisson and Zotkina, 2015). For digitizing small objects, it is necessary to use macro lenses, extension rings or zoom lenses ensuring large-scale photographs, e.g. 1:1 or larger, with the minimal distance between the camera and the object. The 1:1 scale means that one photo captures an area, equal to the digital camera's image sensor size. The main difficulty of the macrophotography is connected with a small focus range (Gajski et al., 2016). However, there are advanced technologies and methods which allow to overcome this restriction by means of generation of composite images from a set of images made with varying focus (Gallo et al., 2014; Kontogianni et al., 2017), or at various distances from the object (Kazakov et al., 2016).

We have chosen the digital photogrammetry technology SfM for the 3D digitizing of full-scale rock surfaces with high resolution. It is the optimal solution ensuring high mobility and autonomous operation of the equipment.

## 3. METHODS AND EQUIPMENT

### 3.1. Control and analysis of the previous work

During implementation of the project on digitizing Old Turkic runic inscriptions in 2017, we have used a rock surface digitizing method involving the technology of macrophotography and digital photogrammetry with the resolution sufficient for documenting the micro-relief of a surface in order to identify runic signs (Vavulin, 2017). In the course of laboratory tests of the accuracy of the 3D models achieved with the program Agisoft Photoscan (v. 1.4.2), we have made a series of experiments with the Nikon D700 camera with the Sigma 105 mm 1:2.8 DG MACRO HSM macro lens.

In order to calculate the maximal resolution of the model when using the macro lens, it is more reasonable to operate with the scale value that is 1:1 at the minimal shooting distance for the lens used. With that, the Ground Sample Distance will be directly proportional to the physical size of the camera's image sensor and inversely proportional to the image scale value:

$$GSD = \frac{l_s}{M \times l_{px}}, \quad (1)$$

where

*GSD* – Ground sample distance,

*M* – Image scale,

$l_s$ – Camera's image sensor length,

$l_{px}$ – Image length (in pixels),

$\frac{l_s}{l_{px}}$ – Size of one sensor on the matrix.

The used camera features the 36×24 mm full-frame matrix with 4256×2832 pixels image resolution (12 MP). According to the formula (1), the Ground sample distance (GSD) which may be ensured by this equipment is approximately 8.5 μm. Artec Spider 3D scanners with maximal resolution up to 0.1 mm and accuracy up to 0.05 mm, were used for the quality control.

For testing the local accuracy, the digitizing area was restricted to one frame coverage (36x24 mm). A shooting scenario with parallel shift of the camera was used; it was implemented during digitizing the rock surfaces. One reference cylinder with the diameter 6 mm and height 1 mm was placed on the reference plane. The camera was installed on the photo slider with horizontal marking in order to ensure precise shift distance. The slider was installed on the photographic tripod with vertical shift marking. For this shooting scenario, it is necessary to ensure a minimally 70% overlapping of the photos by the horizontal shift of the camera and 50% by the vertical camera shift. In our case, the camera was shifted each time by 1 cm, first horizontally, until the end of the line, and then vertically, to the next line of shooting. In the result of the images' processing using the standard settings of the software, a correct aligning of the photos and calculation of points' coordinates have been achieved. However, the calculated points' height has proved to be much less than their true height, by approximately 2.8 times.

The used lens has an optical system, different from that of the standard 50 mm lenses. In such cases, an additional calibration of the camera and the lens may be required (Percoco et al., 2015). The standard calibration means of the camera, Photoscan, have not given the desired effect. The use of similar lens has shown good results of surface projection in the course of a circular shooting scenario while digitizing a small-size object (Clini et al., 2016). A use of the automatic calibration data obtained during model generation have also not had the desired effect for the camera calibration in our case. Using the photos made with the parallel camera shift, we have failed to achieve a correct surface projection in the Agisoft Photoscan software. This was probably related to specific construction features of the used macro lens and its possibility of focusing when shooting an object from a very close distance. Its optical characteristics do not correlate with the standard optical ratios expressed by the thin lens formula (2).

Consequently, the data obtained in the year 2017 have proved to contain height errors. Our assessments of the cuts' depth in the earlier published works was erroneous (Vavulin, 2017; Nevskaya et al., 2018; Vavulin et al., 2018). Although 3D models with high resolution were generated as a result of the work in 2017, they contained height errors. Nevertheless, the obtained results were sufficient for the determination and identification of various cuts on the rock surface (including their identification by the relative cuts' depths), and for the recognition of the runic signs. Since the primary goal (high-detailed documentation of the runic signs and their reading) has been achieved, a repeated shooting of these surfaces is not required.

### 3.2. *Method development*

#### 3.2.1. Macrophotography theory

Another hardware-based solution for implementation of macrophotography is the use of extension rings. Their use along with the standard fixed focus lens will fully correspond to the optical ratios described by the thin lens formula that should be used for the photographic calculations:

$$\frac{1}{u}+\frac{1}{v}=\frac{1}{f}, \quad (2)$$

where

$u$ – Distance from the lens to the object (object distance),

$v$ – Distance from the lens to the image (image distance),

$f$ – Focal length.

From this ratio, the unknown values may be calculated using the two known values accordingly:

$$u=\frac{f\times v}{v-f}, \quad (3)$$

$$v=\frac{f\times u}{u-f}, \quad (4)$$

The total shooting distance will correspond to the distance from the object to the camera matrix:

$$D=u+v, \quad (5)$$

where

$D$ – the total shooting distance.

The total shooting distance can be measured manually or using the minimum lens focal length value in conditions of shooting with the maximum possible approaching to the object. By expressing the object distance (u) or the image distance (v) via the total shooting distance (D) we obtain the reduced quadratic equation, the roots of which represent the target values:

$$u,v=\frac{D\pm\sqrt{(-D)^2-4fD}}{2}. \quad (6)$$

The scale of the obtained image will be equal to the ratio of the image distance to the object distance and it will be described by the linear magnification formula or it may be expressed via the lens focal length:

$$M=\frac{v}{u}, \quad (7)$$

$$M=\frac{v}{f}-1. \quad (8)$$

The extension rings move the lens away from the camera matrix physically increasing the image scale with the focal length (f) remaining constant:

$$M_2=\frac{v+b}{f}-1, \quad (9)$$

where

$M_2$ – Scale of the image obtained with the use of the extension rings;

$b$ – Length of the extension rings.

Thus, it is possible to calculate the rings length (b) required for obtaining the target scale ($M_2$) using one of the following formulas in accordance with the known parameters:

$$b=f\left(M_2-M\right), \quad (10)$$

$$b=f\left(M_2+1\right)-v, \quad (11)$$

The AF Nikkor 50 mm 1:1.8 D fixed focus lens with minimal focusing distance 420 mm was used. By the maximal approaching to the object, the object distance and the image distance are 362 mm and 58 mm respectively, see formula . (6). According to the formulas (7) and (8), this lens at a minimal distance generates an image on the matrix with the scale 0.16 or 1:6.24. In order to obtain the scale 1:1 it is necessary to move the lens away from the camera by 42 mm according to the formula (10). Out of the set of the three extension rings (12, 20 and 36 mm high) that we had at our disposal; we have assembled a system with the total extension of 48 mm (out of the 12 and 36 mm rings). With this extension, the scale of the obtained image is equal to 1.12, according to the formula (9). According to the formula (1), the maximal resolution, i.e. ground sample distance (GSD), is equal to approximately 7.5 μm.

Besides, the depth of field is significantly reduced when the extension rings are used. With such magnification, it is necessary to take into account the maximal possible depth of field even when shooting flat objects. It depends on the focal length of the lens, distance to the shooting object, the f-number and the circle of confusion, which shall not exceed the camera's matrix sensor size. In order to calculate the possible depth of field it is necessary to find the values of the near and the far limits of the sharply imaged space (Kraus, 2007: 58-62):

$$u_{n,f} = \frac{u \times f^2}{f^2 \pm f_n \times c \times (u - f)}, \quad (12)$$

where

$u_n$ – Distance from the lens to the near limit of depth of field,

$u_f$ – Distance from the lens to the far limit of depth of field,

$u$ – Distance from the lens to the focusing point (the object),

$f$ – Lens focal length,

$f_n$ – f-number,

$c$ – The circle of confusion diameter limit.

The distance located within the calculated limits will represent the maximal possible depth of field (Gajski et al., 2016):

$$P = u_f - u_n, \quad (13)$$

where

$P$ – Depth of field.

For a lens with 50 mm focal length with a 48 mm set of the extension rings (with v = 106 mm) the minimal distance from the lens to the focusing point (u) according to the formula (3) will be equal to 94.64 mm. The maximum f-number of the lens used is 22 units. The sensor size of the Nikon D700 camera matrix is 8.5 µm (1). Accordingly, this size represents the circle of confusion diameter limit. Using these parameters and in accordance with the formulas (12), (13), we obtain the depth of field equal to only 0.632 mm even with the minimal relative aperture. Such small depth of the field assumes shooting only with the lens aperture closed to the maximum. Even in this case many of the areas falling outside of this range will be blurred. We did not use any additional methods for increasing the depth of field at this stage of the works.

Another specific feature of the macro rings usage is represented by a reduction of the exposure value. Along with the necessity to use the lens aperture closed to the limit, this leads to a significant darkening of the photograph. Higher ISO speed values, slower shutter speed or flash may be used for the exposure compensation.

### 3.2.2. Local accuracy control

Then the test photographic recording of a wooden panel was carried out under the same scenario as in the first test – with horizontal camera shift by 1 cm along the shooting line and consequent vertical shift of the line of shooting by 1 cm. 12 photos were taken for recording the area containing the reference cylinder. Slower shutter speed (up to 15 seconds) was used for exposure compensation in the laboratory conditions.

The obtained data was processed with various camera calibration parameters in order to get the best result. The generated models were compared to the scanning data (Artec Spider scanner) for accuracy verification.

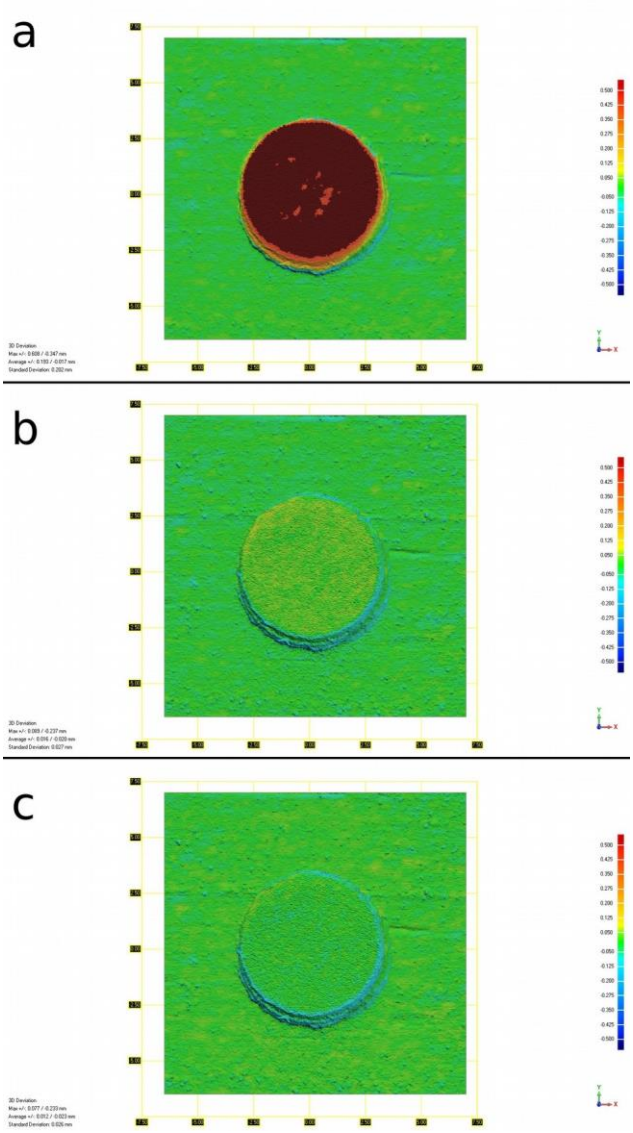


*Figure 2. Comparison of the reference area of the model achieved by scanning (resolution 0.1 mm, accuracy 0.05 mm) with the models generated using the photogrammetry method as the result of the tests: a – automatic calibration, b – standard manual calibration, c – use of the automatic calibration under the circular shooting scenario.*

With automatic calibration, the height of the reference cylinder in the reconstructed model was approximately 2.9 times less, and the maximum deviation exceeded 0.6 mm – the same results as with the use of the macro lens (Fig. 2a). With manual camera calibration using the standard means of the Agisoft Photoscan software, the deviations from the reference model reached 0.089 mm. This value reflects to the geometry inflection area on the cylinder edge. The deviations not exceeding the 3D scanner resolution (0.1 mm in our case) can not be measured accu-

rately in this area. A true error exceeding the scanner accuracy (0.05 mm) on the flat area of the object was observed only in a small area on the cylinder edge (Fig. 2b). Small areas located along the entire plane where the deviations exceed the 0.05 mm reference value represent the geometry elements with size less than 0.1 mm which is outside of the 3D scanner resolution range and which are absent in the reference model. In the third case, the automatic lens calibration data was used which was obtained during separate object processing under the circular shooting scenario. In the third case, a model was generated where large geometry areas with deviation from the reference model exceeding 0.05 mm were absent. (Fig. 2c). As a result, the model with resolution up to 0.0075 mm and accuracy not less than 0.05 mm was generated.

### 3.2.3. Global deviations control

In general, the capabilities and accuracy of digital photogrammetry using different cameras and software have already been tested (Georgopoulos, 2016; Niederheiser et al. 2016). However, for the specific survey technique presented here, a separate check of global distortions was required.

Beside the local accuracy control, a global deviations' control is also required when a large area is digitized. A 64 x 32 cm (0.2 m²) wooden panel with the Creaform 3D scanners' positioning markers was used for the test digitization. During the selection of a photography method ensuring the least global deviation of the surface, three sets of photos were taken and four options of data processing were used.

The first option included only the macrophotography that was carried out using the 50 mm lens and the extension rings installed to reach the total length of 48 mm. In total, 1841 photos were taken for the test panel covering with camera horizontal shift by 1 cm and vertical shift of the shooting line by 1 cm. In the second case, 27 large-scale images were added to the basic macro photography that were taken using the 50 mm lens only. The photos were taken from the minimal shooting distance of 42 cm with parallel camera shift and at least 70% image area overlapping. In the third case, the general view photos of the entire panel were added to the basic macrophotography. These photos were taken using the 50 mm lens only in such a way that the entire plane was covered by the frame overview area from seven different perspectives with radial displacement. In the fourth case, all three data sets – 1841 macro photos, 27 large scale photos and 7 general view photos were used. Separate calibration groups were set up for the macrophotography, large-scale photography and the general view photography. The calibration was set in advance for the macrophotography group only, but it was not fixed. The adaptive camera model fitting function was enabled during the photos' alignment. The Creaform GoScan 3D scanner with the maximal resolution up to 0.5 mm and accuracy up to 0.1 mm was used for the global deviation control accuracy check. Coordinates of the checkpoints obtained by the 3D scanning of the plane were compared with the coordinates calculated during the model reconstruction using the photos. In total, 15 checkpoints were located on the plane. In order to consider the possibility of the method application without the expensive 3D scanner, the checkpoints were not used as the reference control points, which would almost completely compensate the global deviation of the model.

As the result of deviation control, the following data on the model deviation ware obtained with the use of various sets of photos (Table 1). The obtained results show that when only the photos taken with the extension rings are used the radial deformation of the overall surface takes place with concave plane center (Fig. 3a). Deviations on the control points reach ±4 mm. When the large scale photos are added to the recording, the radial character of deviation remains but the plane is incurved in the opposite direction and its center becomes dome shaped (Fig. 3b), with the increase in absolute values of deviations up to ±5.5 mm. When the general view photos are used together with the macrophotography images, deviations of the model are analogous to the second option – radial deviation with dome shaped center, but the deformation level is significantly lower – ±2.5 mm (Fig. 3c). In the fourth case, when all three sets of photos are used, the radial shape of deviation remains similarly to the first test, with the concave center (Fig. 3d), but the deformation magnitude is considerably less. Deviations on the control points do not exceed ±0.3 mm. The obtained errors of the control points on the plane are similar to the height errors (according to the radial shape of deformation), and do not exceed ±0.3 mm.

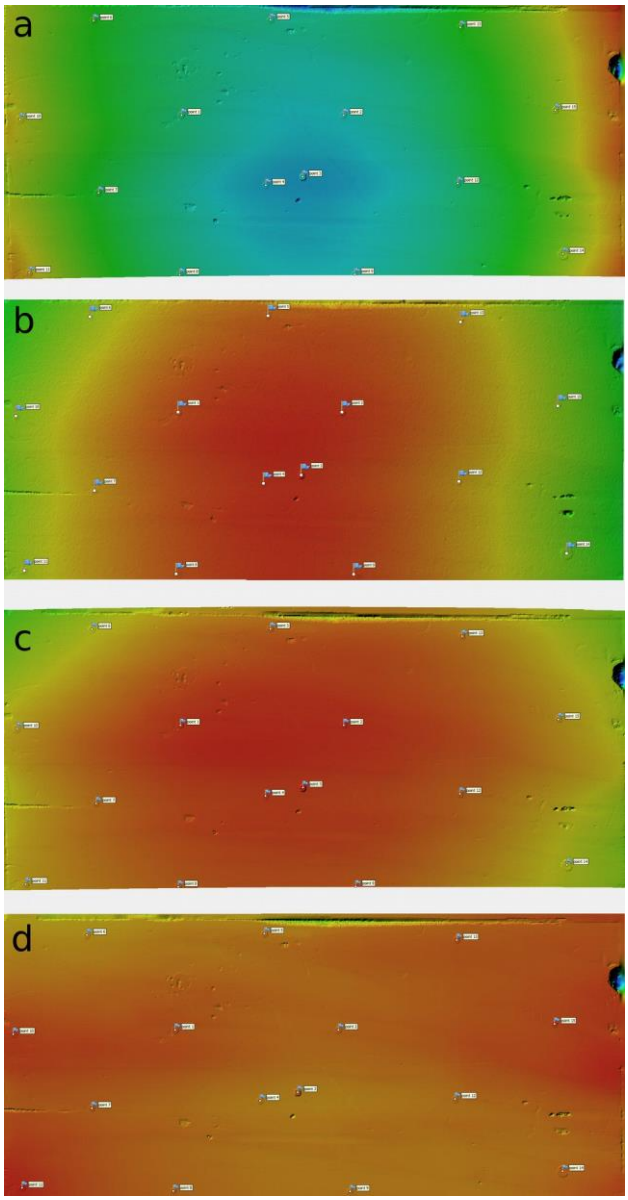


*Figure 3. Height map of the control plane and its deformations corresponding to different data sets used: a – only macro photos (50 mm lens + 42 mm of extension rings), b – macro photos + large scale photos, c – macro photos + general view photos, d – macro photos + large scale photos + general view photos.*

### 3.2.4. Method development result

This method allows for 3D reconstruction of the planar object with high resolution with the use of the extension rings for image magnification in the Agisoft Photoscan software. Using the 50 mm lens together with the 48 mm extension rings allows obtaining an image /with the scale slightly exceeding 1:1. The final resolution depends on the parameters of the camera used. In order to get a set of macro photos, it is necessary to ensure precise parallel shift of the camera approximately by 30% of the view area both horizontally and vertically. With scales like these, the use of auxiliary equipment in order to ensure regular and precise shift (photo slider, photo tripod or another equipment) is mandatory. For minimizing the global deviation of the entire object's model, three sets of photos are required:

1. macrophotography (the closest distance for the 50 mm lens with 48 mm extension rings, taken with parallel shift of the camera);
2. large-scale photography (the closest distance for the 50 mm lens with parallel shift of the camera);
3. general view photography (shooting with the 50 mm lens when the object fits entirely into the view area of each frame, with radial shift of the camera).

A special calibration of the camera with the optical system used for the macrophotography (lens and extension rings) prior to the data processing is mandatory. In this way, we have achieved the resolution of 0.0075 mm with the local measurement accuracy not less than 0.05 mm, using the Nikon D700 camera. In order to obtain the necessary set of macro photos, we have used the camera shift by 1 cm horizontally and by 1 cm vertically. The maximal global deviation of the achieved model of the entire plane has been up to 0.3 mm.

***Table 1. Deviations of the control points of the generated models in height from the scanning data (mm). The processing sets consisted of the following photos: 1841 macro photos, 27 large scale photos and 7 general view photos.***

| Control point number | 1st set (1841 photos) | 2nd set (1841 + 27 photos) | 3rd set (1841 + 7 photos) | 4th set (1841 +7 + 27 photos) |
|---|---|---|---|---|
| 1 | -2.066 | 3.101 | 1.837 | -0.059 |
| 2 | -3.979 | 4.438 | 2.1 | -0.265 |
| 3 | -3.615 | 5.405 | 2.636 | -0.109 |
| 4 | -3.427 | 5.241 | 2.319 | -0.208 |
| 5 | -1.717 | 3.183 | 0.907 | 0.001 |
| 6 | 2.088 | -2.192 | -1.36 | 0.027 |
| 7 | 0.501 | 0.214 | 0.208 | 0.078 |
| 8 | -1.744 | 3.19 | 0.852 | -0.124 |
| 9 | -2.464 | 4.503 | 1.437 | -0.113 |
| 10 | 3.864 | -5.04 | -1.934 | 0.231 |
| 11 | 3.98 | -4.406 | -2.04 | 0.099 |
| 12 | -1.12 | 0.754 | 1.027 | -0.024 |
| 13 | 0.619 | -0.209 | -0.257 | 0.028 |
| 14 | 3.67 | -4.907 | -2.153 | 0.228 |
| 15 | 2.987 | -4.844 | -1.473 | 0.136 |

### 3.3. *Field tests*

Field tests of the developed method were carried out in 2018 (Fig. 1) within the frames of the continued works on the 3D digitizing of Old Turkic runic inscriptions of the Altai Mountains. In course of the work, seven planes containing runic inscriptions were documented (Table 2). In all cases, the developed method was used in conjunction with the equipment described above (Fig. 4). Additionally, 3D scanning of all planes was carried out in order to control the global deviation of the whole model (Creaform GoScan 50) (Fig. 5), and two planes were scanned with high resolution for the local accuracy confirmation (with the scanner Artec Spider).

This method requires taking large number of photos, approximately 10-11 thousand per square meter. Accordingly, it takes a lot of time. During testing of the method, the speed of 15 hours per 1 m$^2$ was achieved, but this was true only for the ideal conditions of equipment installation.

***Table 2. Data collection during the fieldwork in 2018.***

| Name | Area (m$^2$) | Photos | Time (hr : min) | Shooting speed (hr/m$^2$) |
|---|---|---|---|---|
| Tumchuk Koby I (A - 95) | 0.091 | 873 | 3:24 | 37.4 |
| D'odro I | 0.08 | 1037 | 4:59 | 62.3 |
| Kurgak I (A - 78) | 0.203 | 2051 | 6:06 | 30.0 |
| Bar-Burgazy I (A - 18) | 0.049 | 507 | 1:38 | 33.3 |
| Bichiktu-Boom VI (A-95) | 0.061 | 681 | 1:50 | 30.1 |
| Karban IV | 0.144 | 1454 | 2:08 | 14.8 |
| Karban I, II (A-50) | 0.09 | 1047 | 3:18 | 36.7 |

***Figure 4. Recording of a surface with runic symbols.***

***Figure 5. 3D scanning of the surface for deviation control of the final model.***

We were faced with some difficulties during the field tests. First, in the daylight (when taking photos in shadow) the exposure is not sufficient for ensuring the fast shutter speed even with the elevated ISO values. The use of the slower shutter speed is complicated by instability of the "tripod – slider – camera" system. After each camera shift, it is necessary to wait for some time until the system stops weaving in order to get sharp images. During windy weather, this approach is not applicable at all. Besides, the use of a slower shutter speed will slow down our, already low, recording speed. In order to resolve this problem, it is possible to use constant artificial illumination or flash. During the fieldwork of the year 2018, we used the Raylab R-10 TTL macro flash be-

cause a portable source of the constant artificial illumination was not available, although the use of flash during object recording for digital photogrammetry is not recommended (Agisoft, 2018).

The second problem is related to the limitations in the equipment installation in the field. Since the recording must be carried out from a very close distance (about 9.5 cm), difficulties may arise with the tripod installation due to the stones protruding at the cliff base. Also, difficulties may be encountered when installing the slider if the surface with runic inscriptions is located in a recession as compared to the common plane of the rock. The whole system is restricted in height by the maximal height of the tripod. For recording the objects located lower, we used vertical installation of the slider or the expedient means ensuring accurate vertical shift by approximately 1 cm.

Each recording was processed in the Agisoft Photoscan software (v. 1.4.4) in accordance with the following procedure: import of the photos, their distribution by calibration groups (3 groups) of the camera, camera calibration import for the macrophotography group, photos alignment process. In case non-aligned or incorrectly aligned photos were present, the alignment process for such photos was repeated using the already determined feature points. After successful alignment of all photos, scaling of the model and orientation of the surface with runic inscriptions in relation to the XY plane of the local coordinates system were carried out. Then the photos of the second and the third groups (large scale shooting with 50 mm lens and general view photos shooting) were blocked and excluded from further processing. The entire reconstruction region was split into chunks, i.e. approximately 10 × 10 cm squares with 1% overlapping using the script software (Agisoft, 2017). Further processing was carried out in the batch process mode. For each chunk, an ultra-high quality dense cloud with aggressive depth filtering, a digital elevation model (DEM), and an orthomosaic were built. Due to the difficulties of working with the large volumes of data in the third-party applications, the 3D data themselves (point clouds or polygonal models) were not used any further. The DEMs and orthomosaics exported in the GeoTiff format were used for further work.

### 3.3.1. Global deviations control

The coordinates of the control points extracted from the scanning data (Creaform GoScan 50) were imported into the Photoscan project for control of the global deviation of the model; deviations from the coordinates calculated using the photogrammetry were detected (Table 3).

***Table 3. Global deviations of the entire plane models.***

| Name | The greatest measurement of the plane (mm) | Number of control points | The greatest error in the plane (mm) | The greatest height error (mm) |
|---|---|---|---|---|
| Tumchuk Koby I (A-95) | 420 | 9 | 0.39 | 0.78 |
| D'odro I | 450 | 8 | 0.17 | 0.56 |
| Kurgak I (A-78) | 920 | 11 | 1.13 | 0.35 |
| Bar-Burgazy I (A-18) | 630 | 10 | 0.19 | 0.97 |
| Bichiktu-Boom VI (A-95) | 370 | 9 | 0.26 | 0.76 |
| Karban IV | 580 | 18 | 0.27 | 0.53 |
| Karban I, II (A-50) | 400 | 18 | 0.32 | 0.67 |

As a result of testing the method accuracy during the fieldwork, we can state that the global deviation of the models is greater in field than in the laboratory conditions. Additionally, in all tests the radial deformation with a concave center is present. Thus, the greatest errors fall within the limits of ±1.2 mm in the horizontal plane and ±1 mm in the height. Whereby in all tests the greatest errors are encountered in the points located at the edge of the recorded area. This can be explained by the radial shape of the deformation, and, in some cases, by a smaller number of the photos. On an average, the surface deformation does not exceed the ±0.7 mm limit both horizontally and vertically.

### 3.3.2. Local accuracy control

For the local accuracy control, models of the planes D'odro I and Bichiktu-Boom VI were built with the resolution 0.1 mm, maximal for the Artec Spider 3D scanner. However, these models were not used entirely for the local accuracy control, as they also featured global deviation up to ±1 mm as compared to the Creaform GoSnan 50 3D scanner data (Fig. 6). This is related to specific features of the

scanner which were evident when scanning objects exceeding its field of view (180 × 140 mm) without the use of additional methods (Vavulin et al., 2014). Small areas with runic signs were used for comparison. One sample was taken from the model built using the 3D scanner and the other was cut out from the dense cloud obtained using the photogrammetry and converted into a polygonal 3D model (Fig. 7). The comparison was carried out using the Geomagic Wrap software. Since the declared accuracy of the Artec Spider 3D scanner is 0.05 mm (Artec, 2019), deviations less than ±0.05 mm were not taken into account during the models comparison (Fig. 8). Maximal deviations did not exceed the 0.1 mm limit in small areas with maximal diameter 0.3 mm, which rather confirmed that the error occurred due to insufficient resolution of the scanner. Deviations in the main area did not exceed the ±0.05 mm limit. Thus, the proposed method ensures the 0.05 mm minimum local accuracy of the built model.

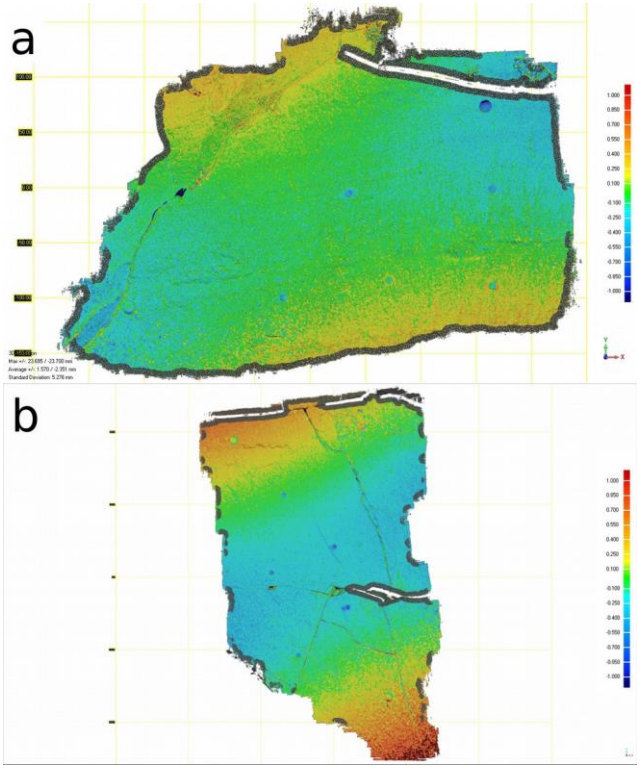


*Figure 6. Global deviation of surface of the 3D model built with the Artec Spider without the use of any special methods in comparison with Creaform GoSnan 50 3D scanner data. The highest deviation of these models is up to ±1 mm.*
*a – Bichiktu-Boom VI plane, b – D'odro I plane.*

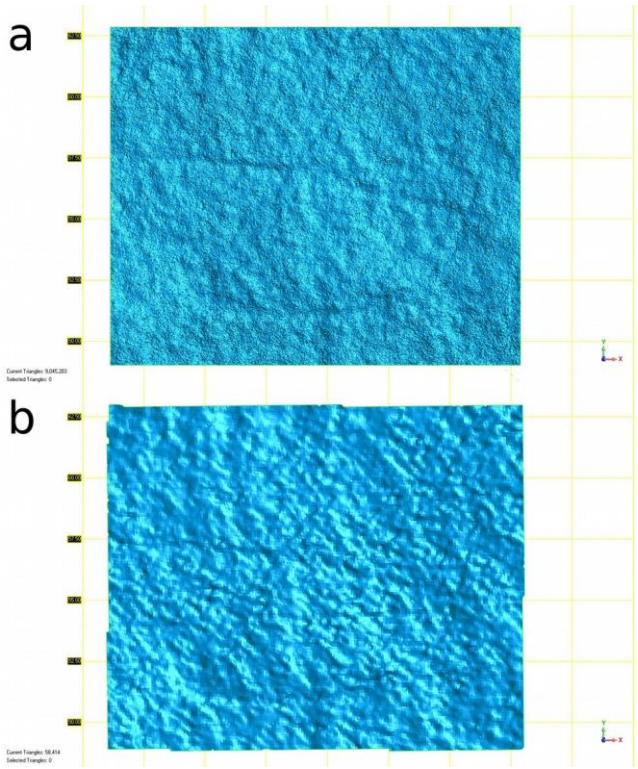


*Figure 7. 3D models of the area with one runic sign: a - photogrammetry (resolution 0.0075 mm), b - 3D scanning (resolution 0.1 mm).*

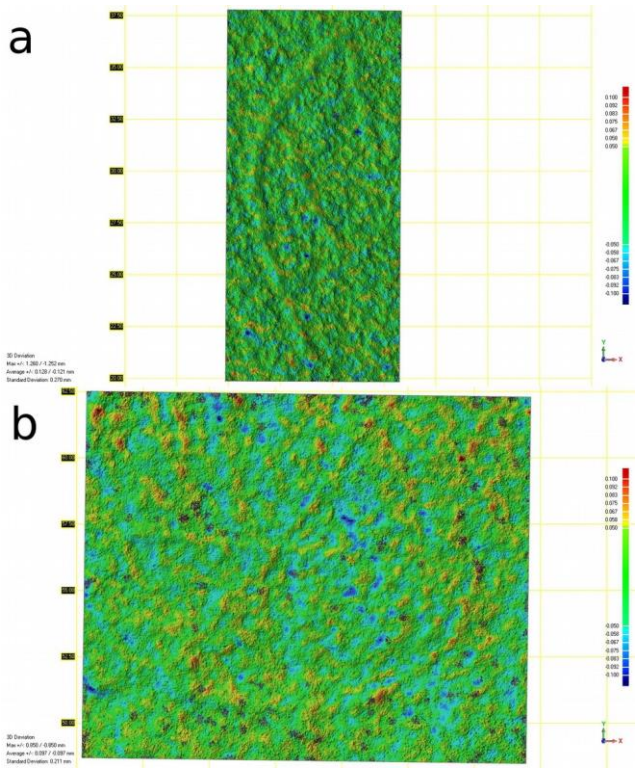


*Figure 8. Local accuracy control for the built models: a - D'odro I, b - Bichiktu-Boom VI.*

### 3.3.3. Field testing results

The following can be concluded based on the field-testing results. The developed method allows for successful obtaining of the 3D data of the whole surfaces with resolution up to 0.0075 mm (with the equipment used), with the local accuracy over 0.05 mm and the global deformation of the entire area not exceeding 1.2 mm (from the distance of 920 mm from the documented surface). Additionally, the necessary hardware is quite lightweight and may be organized as a mobile package for delivery on foot, which ensures possibility of working in the hard-to-reach places. However, this method requires a lot of time for the field data collection (over 15 hours per one square meter). Its use is restricted by the possibility of the physical installation of the equipment near the documented surface, which in some cases may not be feasible. Besides, in order to obtain the best documentation results, an additional fixed light source is required for taking photos.

## 4. ANALYSIS OF THE PROCESSED DATA

The output data (height maps and orthophotos) are optimized for working with the geographic information systems (GIS). The QGIS software was used for the surface analysis and for depicting lines. The achieved height maps were imported into the project with three different settings. First, the height map layer in the Singleband gray render type with an automatic gradient stretching to the extremum values in the visible area for the main detailed analysis of the relief (Fig. 9b). Second, the height map layer in the Hillshade render type for viewing the details clearly distinguished in the relief simultaneously in the entire plane (Fig. 9c). Third, the height map layer in Hillshade render type laid over the orthophoto in the "soft light" blending mode for the creation of a shadow on the orthophoto and the simultaneous analysis of color and relief of the surface (Fig. 9d).

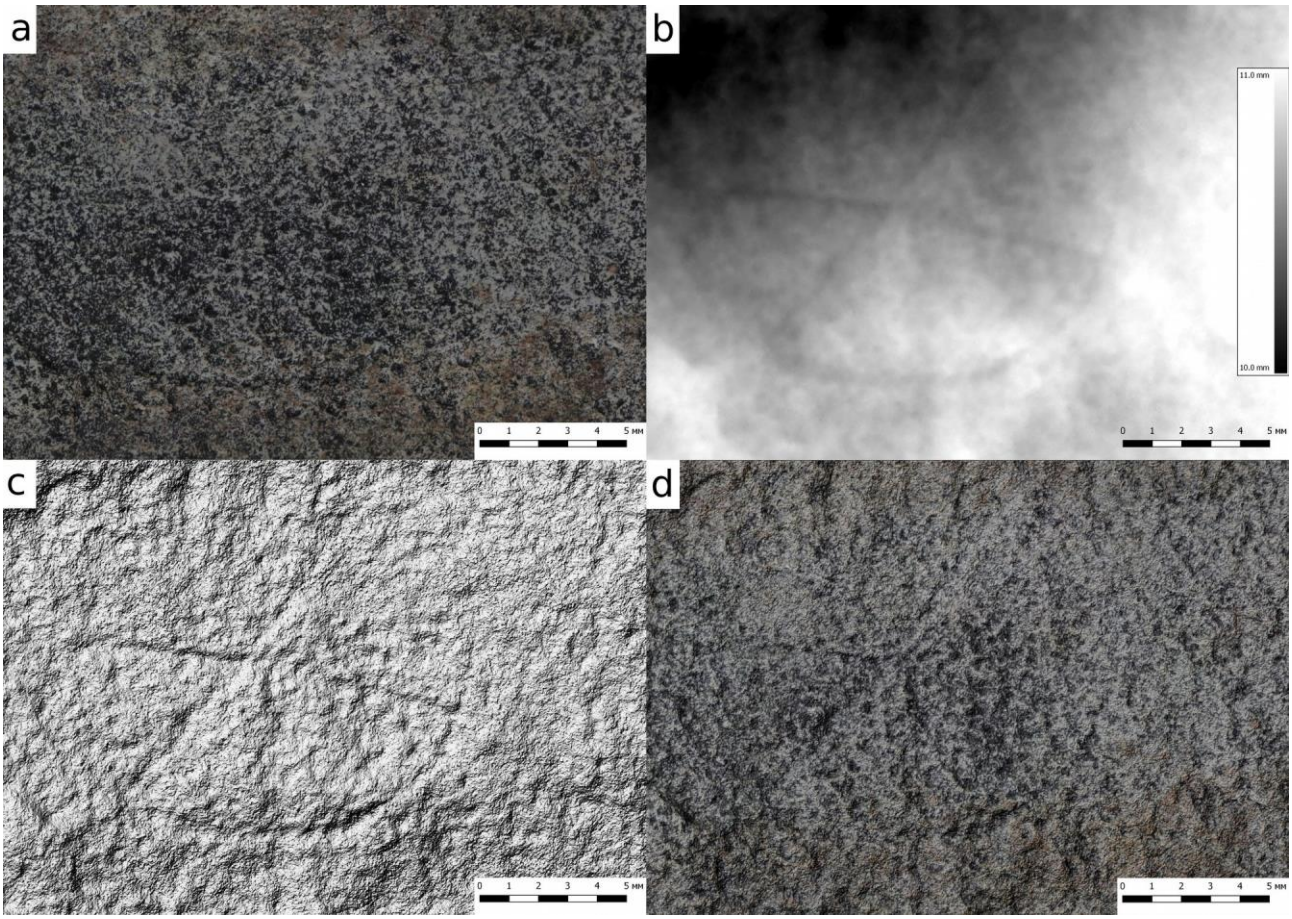


*Figure 9. Layers for working in QGIS: a - orthophoto, b - height map, c - height map in the Hillshade render type, d - height map in the Hillshade render type and in the "soft light" blending mode laid over the orthophoto.*

### *4.1. D'odro I*

The D'odro I inscription is located near the Chuya Route, 3.8 km from the D'odro village (the Onguday Region of the Republic of Altai) in the direction of the Inya village. This horizontal inscription was found by B. M. Kindikov in 2009 (according to the information received from the discoverer). Boris M. Kindikov has published very schematic copies of 2 petroglyphs located on this cliff and depicting a deer above the inscription and an archer below the inscription, as well as 5 runic signs which he could see. However, he could not identify 3 of them (Kindikov and Kindikov, 2018: 61). In 2018, he showed this inscription to the authors of the article.

#### 4.1.1. Physical parameters of the inscription D'odro I

The inscription is located on the 40 x 25 cm rock surface, placed at the foot of the rocky outcrops in 10 meters from the road at the approximate height of 30 cm (in respect to the lower edge of the plane). The cliff itself is characterized by a homogeneous granular structure that does not allow for distinguishing the lines clearly by difference in the surface color. The inscription is accompanied by two pictures of the Old Turkic time – those of a deer and an archer. Their lines are hardly seen on the orthophoto due to the granular character of the surface and the use of the frontal flash during the photographs' shooting (Fig. 10a). The lines of the pictures and of the inscription are seen on the height map (Fig. 10b).

The lines of the runic signs are clearly distinguished from the lines of the pictures by their position and size (Fig. 11).

The inscription is situated between the front and the back legs of the deer; however, the last four symbols are inscribed inside of the back legs' contour continuing the line of writing of the inscription. Nevertheless, the lines of the runic signs do not cross the lines of the picture, and the end of the inscription ideally fits into the picture contour.

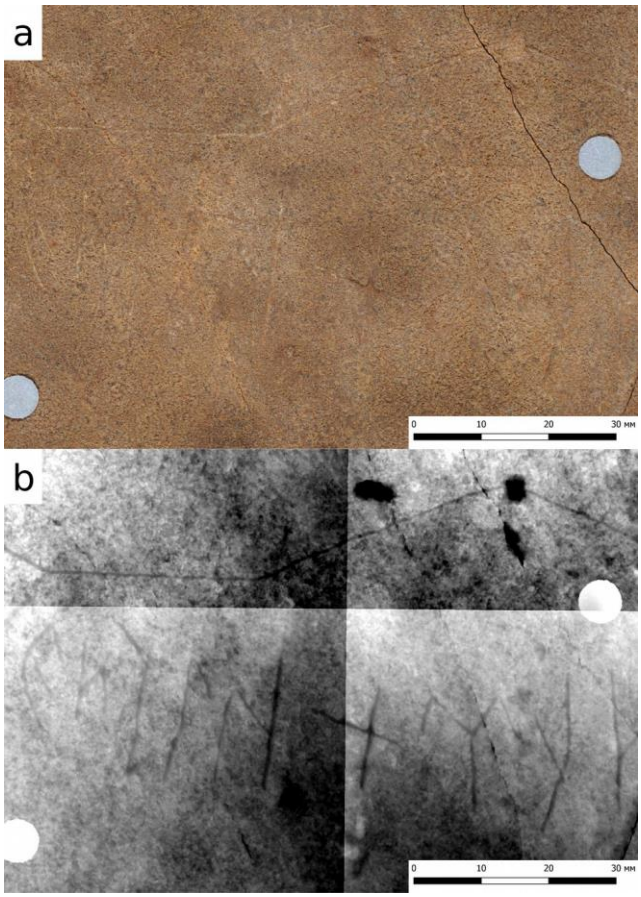


*Figure 10. The surface with the inscription D'odro I: a - orthophoto, b - height map.*

The height of the signs of the main part of the inscription is within the range from 12 to 24 mm, the average characters' height is approximately 20 mm. The last four symbols are significantly smaller, from 8 to 14 mm, and the average height of the characters is about 10 mm. Herewith, both the lines of the runic signs and the lines of the pictures have a similar width and depth; thus, they do not differ in these parameters. The width of the lines is mainly within the range from 0.36 to 0.78 mm, in some places they narrow down or widen within the range from 0.3 to 1.02 mm. In most cases, the depth of the lines is within the range from 0.1 to 0.15 mm. However, sometimes it reaches the range from 0.03 to 0.2 mm. Sometimes, due to the granular surface and the rather shallow signs of the inscription, it is difficult to define clearly, whether a line is artificial, or it represents a natural depression. These cases are segregated into a separate group of lines, and each of them may be a part of the inscription (Fig. 12).


*Figure 11. Lines on the surface D'odro I.*

### 4.1.2. Reading and interpretation of the inscription D'odro I

The reading of this inscription is not quite clear even after the 3D analysis. We have problems with identifying the 7th sign: either it is an irregular A, or it could be an $l^1$ in case we disregard the upper stroke. Consequently, we have at least two possibilities of reading and interpreting this inscription.

Transliteration

$t^2$ ŋ $r^2$ $d^2$ $k^1$ I A/$l^1$ $t^2$ $g^2$ $l^2$ $^{O}$k A $t^2$ $g^2$ $n^2$ A

Transcription

t(ä)ŋr(i)d(ä)k(i) A // t(ä)ŋr(i)d(ä) (a)kïl(ï) // t(ä)glök A t(e)g(i)n A

Translation

'a blind prince in the sky /a prince, whose mind was blinded in the sky / a prince, whose mind was blinded by the sky/God'.

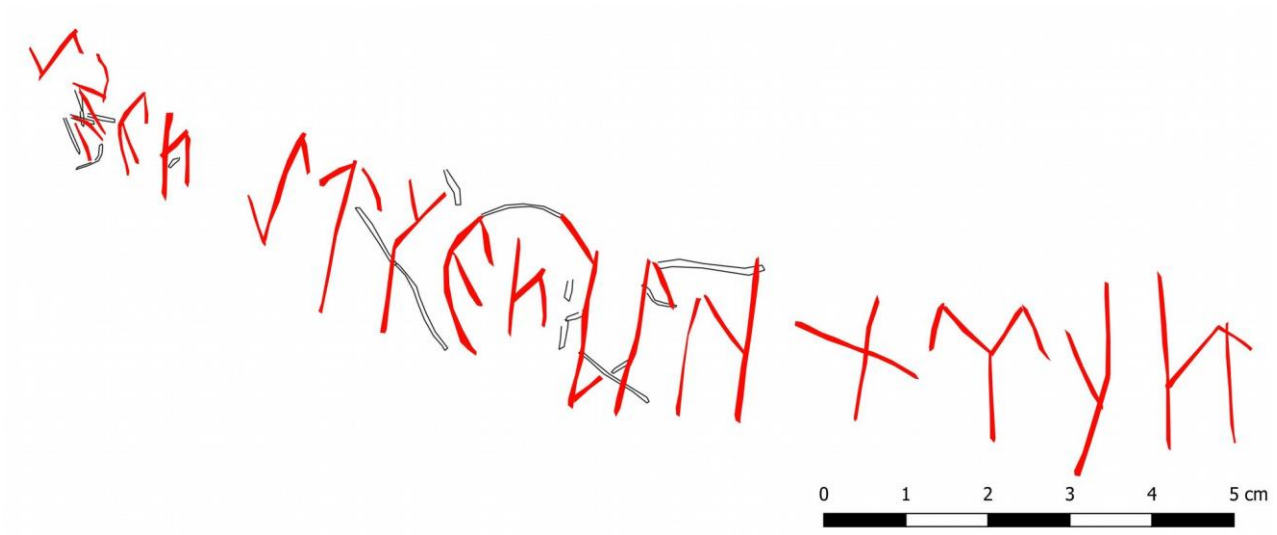


*Figure 12. The runic signs and the non-identified lines of the inscription D'odro I.*

## Comments and Discussion

1. The first four runic signs are seen quite clearly on the rock with "naked eye", contrary to the rest of the signs that could be identified only thanks to the 3D analysis of the surface. The sequence $t^2$ ŋ $r^2$ is undoubtedly read as *t(ä)ŋr(i)* 'god'. The fact that the vowels are not written explicitly is quite common: the first vowel of this word was principally not written explicitly in any Old Turkic sources, in both runic

scripts and in the other ones that had been used to write Old Turkic (Uighur, Manichaean, Sogdian, etc.). The second vowel was normally also not written before suffixes. Here, we have the suffix of the locative case *-dä*, written with the respective consonant only, which might imply that another suffix follows it.

2. We can read the following two signs $k^1$ I as the adjectivizing suffix *–ki*, giving an adjective derived from the noun stem in the locative *t(ä)ŋr(i)d(ä)k(i)* 'being in the sky'. However, this reading needs to be explained. The suffix *–ki* is written with the consonant $k^1$ usually used in words with back vowels while the stem *täŋri* has front vowels. Thus, it is a break of the orthographic rules of the classical runic script, which, however, happens quite often in the Altai variant of this script (Nevskaya, 2011, 2015).
3. *t(ä)ŋr(i)d(ä)k(i)* is followed by the sign A used as an interjection, or just a word divider, the opinions differ respective its function in the Yenisei and Altai runic traditions (Erdal, 2002: 56; Kyzlasov, 2002; Nevskaya, 2011). Thus, we leave the transliteration of the sign in the transcription line. The fact that A is used also after the rest of the words of this inscription, and regularly for this purpose in other Altai runic inscriptions (e.g. Nevskaya et al., 2018; Vavulin et al., 2018), signifies rather its function as a word divider than an exclamation.
   Here, this sign is inverted while its upper stroke is pointing upwards instead of downwards, as compared to the classical form of this sign. This makes the proposed reading questionable. We could think of an alternative reading in case we disregard the problematic upper stroke of A; the rest of the sign would give $l^1$: *t(ä)ŋr(i)d(ä) (a)kïl(ï) t(ä)glök A t(e)g(i)n A* 'A prince whose mind got blinded in the sky'. In this case, we suppose that *(a)kïl(ï) t(ä)glök* is an instance of the so-called *başı-bozuk* (*insan* 'person') construction. The substantivized expression *başı-bozuk* means literally 'one whose head is turned, (with) damaged head, crazy-head' lexicalized as a noun used to define irregular soldiers of the Ottoman army. From the linguistic point of view, in *akïlï täglök tegin*, similar to *başı-bozuk insan*, we have a relative clause, *akïlï täglök*, connected with the head noun *tegin* by mere juxtaposition. The possessive affix on the subject of the relative clause expressing a part of the body of the person denoted by the head noun is coreferent with the head noun: 'the prince, whose mind was/got blinded'.
   Although this second interpretation is also plausible, the fact that we find otherwise A after all the words of this inscription, but not in case of this interpretation, probably, makes the first interpretation more preferable. See more in the section "Discussion".
4. The words that follow seem to be quite clear and are mostly written according to the orthographic rules of the runic script: we interpret $t^2$ $g^2$ $l^2$ $^O k$ *A* $t^2$ $g^2$ $n^2$ *A* as *t(ä)glök A t(e)g(i)n A* 'a blind prince'. The only problem is the use of the sign $^O k$, the so-called 'arrow', in a word with front vowels while it should be used in back-vocalic words in the classical variant of the runic script. However, it is typical that these rules are often violated in Altai runic inscriptions as we have already stated earlier.
   The word *täglök* comes from the verb *tägil-* (*tägil-* formed from *täg-* 'reach' with the passive voice marker *-(I)l*) means primarily 'be reached'; however, it is used nearly always as 'be blinded', i.e. 'reached by some sharp objects' (EDPT: 481). *Täglök* is often transcribed as *täglük* in dictionaries; however, see Clauson (1966: 17) on the vowel of the suffix *-(O)k*). It is a derivative from the verb *tägil-* with the affix *–(O)k* forming nominals (nouns and adjectives) from verbal stems (Erdal, 1991: 224-262). It signifies a subject nominal 's/he who got blinded, the blinded, blind'. Modern Turkic languages use for 'blind' either the Persian loan *kür* (Turkish *kör*), or Mongolic *sokor*, or a periphrasis (EDPT: 480). In Old Turkic, *täglök* was used at all stages and in all varieties (EDPT: 480), see also the VATEC database. In VATEC, it is written without the first vowel in both instances of the use of this word.
   *Tegin* is written without its both vowels, but seems to be quite clear. There is an *A* word divider also after it.
   The form *täŋridä* can mean not only 'in the sky', but also 'by the sky' or 'by the God'. It is well known that the Old Turkic locative *-DA* could also be used in the functions of the ablative case. Since the ablative case can express the source, the reason, the origin of something among many other functions in Turkic languages including the agent in a passive construction, it is possible to interpret *täŋri-dä* here as the agent of the verb *tägil-* 'be blinded'. Then, it is apparently not the sky, but the God acting as an agent in this case.
5. The content of this inscriptions is quite mysterious, no matter which interpretation we pre-

fer. It is interesting that the first interpretation has parallels in another Altai inscription, the Yabogan one (A 84), which has aroused much discussion (Nevskaya, 2016; Sirin User, 2013; Tybykova et al., 2012), in the Chiyin Tash (Ak Öleŋ) inscription in Kyrgyzstan (Alimov et al., 2010; Aydin et al., 2013: 302), and in Yarxoto in China (oral communication with Peter Zieme).

6. The context 'being in the sky' may indicate stars and constellations, as one of the reviewers of the articles has proposed, while 'blinded prince' could mean a Sun or Moon eclipse. However, we are not ready to make any conclusions at present. Being very grateful to the reviewer for this interesting and insightful comment, we will certainly attend to the matter in our future research.

### *4.2. Karban IV*

The location Karban has become a focus of Turcological research only in the recent years. Firstly, the inscription Karban I was discovered by Evgenij Matochkin on the left bank of the river Katun, opposite the village Kuyus in 1988 (Matochkin, 1990). Here, the Karban, an afflux of the Katun River, is flowing into the Katun forming a small valley. The same inscription was rediscovered and published by Vladimir Elin and Vasilij Soenov in 1990 (Elin and Sojonov, 2013).

Then, in 2012, the expedition of Irina Nevskaya and Larisa Tybykova planned to check the signs of the Karban inscription carved on the western wall of a small cave, and its GPS data. Five students of the Frankfurt University took part in the expedition. We use here some of the photos they took during the trip.

On the same side of the cave, Nevskaya and Tybykova discovered further lines that are very much destroyed; therefore, we do not present them here. Still, they should be considered as two further Karban inscriptions. On the opposite side of the cave, Irina Nevskaya and Larisa Tybykova found another inscription consisting of four lines (Karban IV). It remained unnoticed earlier because of a great amount of Cyrillic signs and scratches made on the rock surface with the runic inscription. It seems that they were attempts to destroy it on purpose. In addition, there were big letters made by watercolor. Nevskaya and Tybykova could remove the paint and the runic signs became visible. The inscription was copied with contact methods and studied by Nevskaya and Tybykova. They also proposed its preliminary reading in their lecture at a symposium organized by the Institute of Turcology, the Freie Universität Berlin, in the fall of 2012.

In 2018, the authors of this article documented this part of the rock with 3D methods.

#### 4.2.1. Physical parameters of the inscription Karban IV

The inscription is located on the surface that is 56 x 25 cm in size. The runic symbols on the surface are very poorly seen because the entire surface is scratched allover in all directions. Beside the deep cuts, multiple shallow lines are made in the entire surface area (less than 0.05 mm in depth) and this significantly complicates determination of the runic symbols on the orthophoto (Fig. 13a). Use of the height map allows identifying only the deepest lines. Out of the total number of deep lines, a group of the deepest recent lines up to 0.4 mm in depth (0.15 - 0.2 mm on the average) and up to 1 mm in width (0.4 - 0.5 mm on the average) was distinguished (Fig. 13b). After those lines had been excluded from reviewing, a large number of lines from 0.05 to 0.15 mm in depth remained (Fig. 13c). Those lines displayed the same physical characteristics and could be parts of the inscription, or meaningless lines.

In the lower left part of the surface, we can identify runic signs quite reliably. They form three lines, each 3 cm high. The strokes belonging to the runic characters can be easily distinguished from the others in this area thanks to their position and height (they are fitting into the line of writing) and depth (the runes' strokes are 0,1 – 0,15 mm deep, other strokes are 0,05 – 0,1 mm).

The upper line on the left side of the surface as well as a line on the right are less clear. There are numerous strokes of the same depth and width as the runes in these parts of the surface. We have applied the following procedure for identifying the strokes that could belong to the inscription. At first, we marked all the strokes of the respective depth that traverse the line of writing. After that, the strokes that fit the line of writing or do not go outside it more than 2 cm were copied separately. Inside this group of strokes, we tried to identify the runic symbols. In the upper line of the left part of the surface, we could identify the strokes belonging to the inscription reliably. In the right part of the surface, we could identify two symbols on the left end of the line and the first symbol on the right end quite well. The central part of this line is very much damaged; many strokes traverse or coincide with each other. All the strokes that fit into the line of writing look similarly relevant and could be parts of runic signs. We cannot either exclude them as parts of the runic symbols, or clearly identify them as such (Fig. 14).

### 4.2.2. Reading and interpretation of the inscription Karban IV

In the fall of 2012, Nevskaya and Tybykova proposed a preliminary reading of this inscription in their lecture at the symposium at the Institute of Turcology of the Freie Universität Berlin. This reading was based on their copy of the inscription done with traditional contact methods.

Here, we first present this copy and the preliminary reading of the inscription and then the reading of the inscription based on the 3D data.

#### 4.2.2.1. Reading based on the contact copy made in 2012 (Fig. 15)

The preliminary reading by Nevskaya, I. and Tybykova, L.

Transliteration

1. $t^2$ š I $b^2$ ? $r^2$ $y^1$ $y^2$ $t^2$ $d^2$ I : $t^2$ z $l^2$/ŋ/$^i$č A
2. ? ? $b^2$ $t^2$ $d^2$ m $r^2$(?) z $y^2$/$l^2$ $g^2$ : $b^2$ $k^2$ $n^2$ m
3. $r^2$ ŋ č $b^2$ $t^2$ $d^2$ m
4. $t^2$ ŋ $r^2$ $n^2$

Transcription

1. t(a)š ev … (e)r (a)y y(e)tdi : t(ä)z(i)ŋ A .../ t(ä)z ičä
2. ... b(i)t(i)d(i)m … y(e)g : b(ö)k(ü)n m(i) / b(ö)k(ü)n(ü)m!
3. (ä)r (a)ŋč(ï) b(i)t(i)d(i)m
4. t(ä)ŋr(i)n

Translation

1. a house made of stone … Er Ay (a person name) reached (it) : Hurry up! / Hurry up to get inside!
2. ... I have written. … Is it good today? / (It is) a good day for me!
3. A hunter-man, I wrote.
4. Tengrin.

As seen from the transliteration and transcription, many runic characters could not be identified, or, as is clear now, were identified wrongly, consequently, only separate words could be read. The inscription could not be interpreted adequately as a whole. We have presented here this first attempt of its reading in order to highlight the possibilities of the 3D documentation methods that we have applied last year.

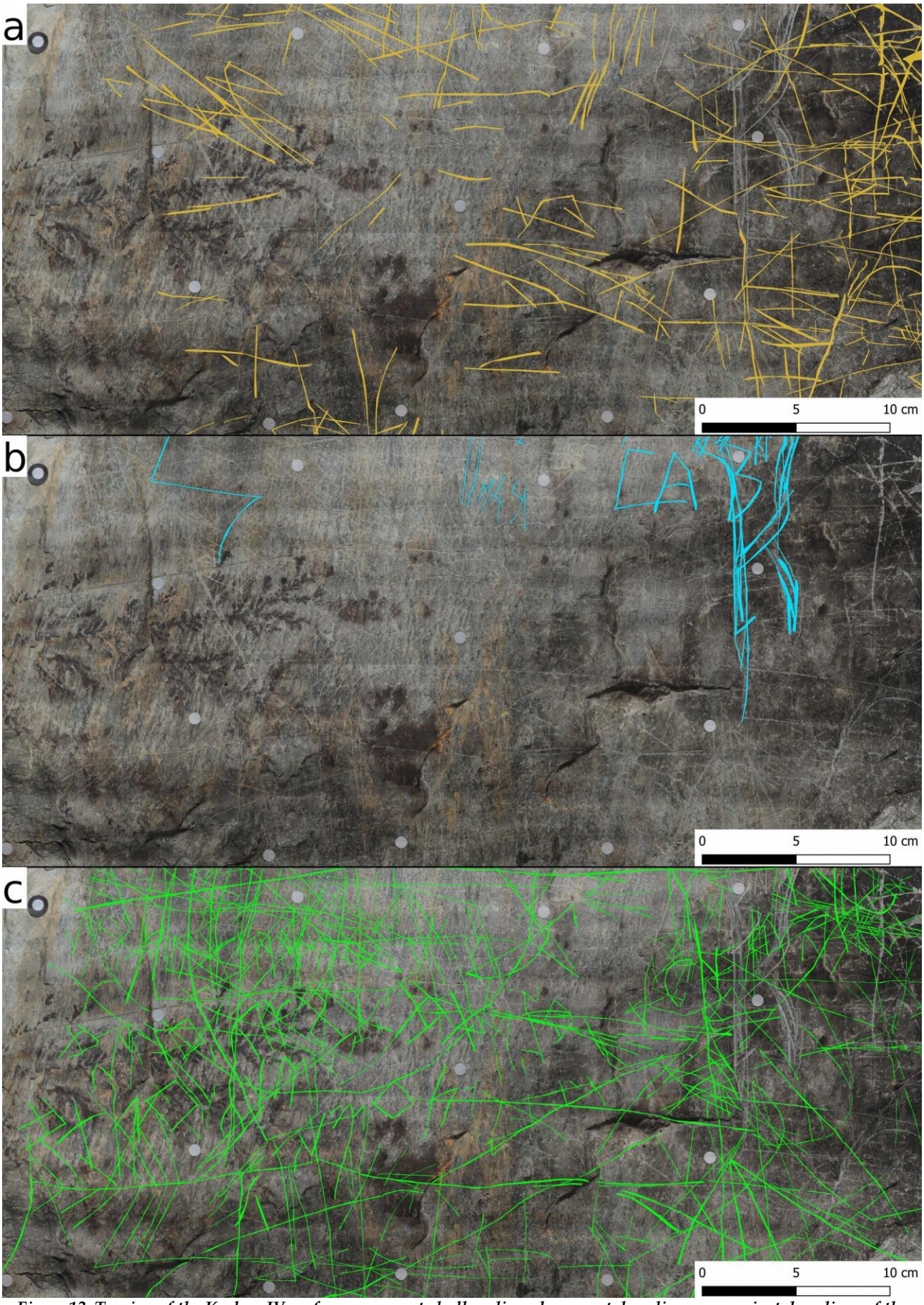


*Figure 13. Tracing of the Karban IV surface: a – recent shallow lines, b – recent deep lines, c – ancient deep lines of the Karban IV surface.*


*Figure 14. Runic symbols and non-identified lines on the Karban IV rock surface.*

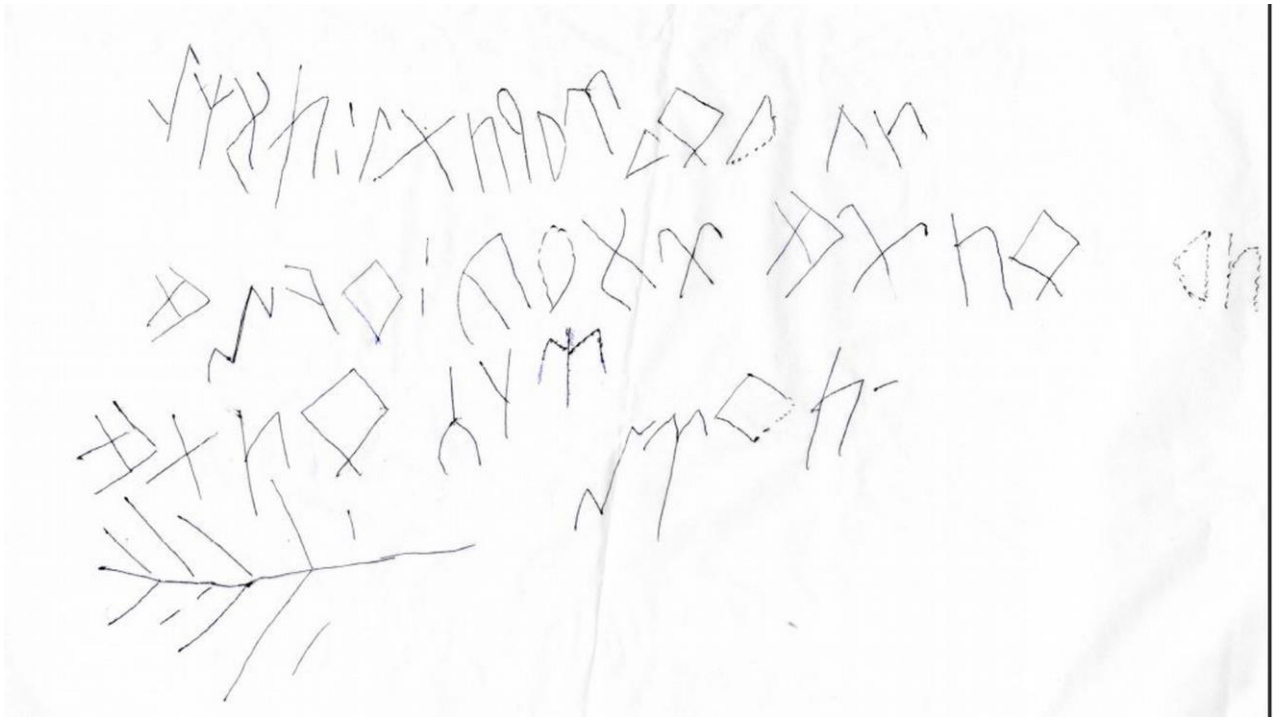

*Figure 15. Nevskaya and Tybykova's copy of Karban IV presented at the Berlin symposium in 2012.*

4.2.2.2. New reading based on the 3D documentation in 2018 (Fig. 14)

Although the inscription remains very difficult for interpreting because of the poor preservation of many characters, we could make some progress in its reading although we are not sure that we have its final interpretation. Thus, we present here again a preliminary one.

The right part of the inscription was impossible to read at all using traditional methods. Now we consider this part to be a separate line, approximately situated at the height of the second line to the right. It could also be possible that it is a part of the second line, but it is not clear then why this line is so much longer than all the rest lines are. It could also be a separate inscription. We start reading the inscription with this separate line.

Transliteration

Right part of the surface:

$b^2$ $t^2$(?) $g^2$(?) $l^2$(?) $g^2$(?) $k^1$(?) $y^1$ A

Left part of the surface:

1. $b^2$ $y^2$ ŋ $g^2$ $y^2$ $t^2$ $d^2$ I : $t^2$(?) z ŋ A
2. :/$s^2$(?) $b^2$ $n^2$ $t^2$(?) $d^2$ m : U/$k^2$ z $l^2$ $g^2$ $b^2$ $k^2$ $n^2$ m
3. $r^2$(?) $r^2$ ŋ č $b^2$ $t^2$ $d^2$ m
4. $t^2$ $b^2$/ŋ $r^2$ $n^2$

Transcription
Right part of the surface:
b(i)t(i)gl(i)g k(a)y(a) A
Left part of the surface:

1. b(a)y (a)ŋ(ï)g // b(ä)y(i)ŋ(i)g // b(o) y(a)ŋ(ï)g y(e)tdi : t(ä)z(i)ŋ A
2. : b(ä)n t(e)d(i)m // s(ä)v(i)nd(i)m : k(ü)zl(ü)g b(ö)k(ü)n(ü)m
3. (ä)r(ü)r (a)ŋč(ï) b(i)t(i)d(i)m
4. t(ä)ŋr(i)n

Translation
Right part of the surface:
A rock with inscription(s)
Left part of the surface:

1. He has killed (lit.: reached) many (lit.: rich) wild animals // He has reached Beying // He has reached this place (side). Hurry up (you all)!
2. : I have written. // I have rejoiced. It is the best day in autumn for me (lit.: it is my autumn day)!
3. (Being) a hunter, I wrote.
4. Tengrin // With (the grace of) the heaven // God.

Comments and discussion

1. The reading of the right part of the inscription is very uncertain because of the difficulties with distinguishing the characters from other strokes on the surface. We read this part: as *bitiglig kaya* 'a rock with inscriptions', which is justified by the fact that there are further runic lines found in this rock cave. The fact that this line is written separately invites to its interpretation as an epigraph to the inscription to the left, or as an address to the sacred rock and the desire to share the information with it. It could be a separate inscription as well.
2. The initial sequence on the left side of the surface $b^2$ $y^2$ *ŋ* $g^2$ $y^2$ $t^2$ $d^2$ I can be interpreted most logically as *b(a)y (a)ŋ(ï)g y(e)tdi* 'He has killed many wild animals', taking into consideration that the inscription seems to be written by a hunter according to the further text. In this case, we have to assume that the character $b^2$, $y^2$ and $g^2$ are used with back vowels, thus violating the classical rules of the runic orthography. However, we know that this happens very often in the Altai runic tradition. Alternatively, $b^2$ $y^2$ *ŋ* $g^2$ *b(ä)y(i)ŋ(i)g* could be the accusative form of the place (or person) name Beying: 'He has reached Beying' /'He has killed Beying (in case it is a person name)' . However, a continuation of these interpretations of the inscription seems to be illogical. Another possibility is that $b^2$ $y^2$ *ŋ* $g^2$ should be read as *b(o) y(a)ŋ(ï)g* 'this side' in the accusative: 'S/he has reached this place (side)', also violating the classical rules of the runic orthography and problematic for a logical continuation.
3. The last word on this line *t(ä)z(i)ŋ* is the imperative form of the second person plural; it can be applied for a polite request to one respected person, or as an address to many addressees: 'Hurry up (you:polite:singular or you:plural)!'
4. The first stroke on the second line could be a lower part of the classical word divider, or the character $s^2$. In the first case, the sequence before the word divider in the middle of this line should be read as *b(ä)n t(e)d(i)m*, in the second case as *s(ä)v(i)nd(i)m*, which is more likely because of the happy circumstances related with the good hunting. In the second variant, we disregard the strokes after $n^2$, marked as uncertain on the copy (Figure ).
5. The final sequence on this line, *k(ü)zl(ü)g b(ö)k(ü)n(ü)m*, is, apparently, a combination of the adjective *küzlüg* formed from the noun *küz* 'autumn' by the suffix *-lXg* (EDPT: 760) and the lexicalized as *bökün* 'today' phrase *bo kün* 'this day' in the possessive form of the 1st person singular. We can translate this phrase as 'the (best) autumn day of mine', literally 'the autumn day of mine', giving no sense here; see Nevskaya and Tazhibayeva (2019) on the use of possessive constructions for expressing superlative semantics.
6. The first character of the third line is apparently $r^2$ written somewhat differently than the consequent $r^2$, although recognizably. It is then the auxiliary verb *är-* 'be' in the aorist form which is a copula part of the nominal predicate *k(ü)zl(ü)g b(ö)k(ü)n(ü)m (ä)r(ü)r*. The word *aŋčï* 'hunter' that we find in some Altai runic inscriptions indicating the creators of those inscriptions, follows it. It can be his profession, or his personal name, although we have not encountered such personal name in other Old Turkic sources. Most likely, it is his profession because the last word of this inscription could be his name.
7. The word on the last line of the left part of the inscription is, most likely, *Täŋrin*, which is used also in other Old Turkic sources as a personal name, probably, a contracted form of *Täŋrikän*. Otherwise, it could be the word *täŋri* 'heaven, god' in the instrumental case expressing also the comitative semantics 'with' giving the following interpretation: with (the grace of) the heaven // God.
8. Alternatively, if we consider the runes to the right of the second line of the inscription to be

the beginning of that line we receive the following reading:

1. $b^2\ y^2\ ŋ\ g^2\ y^2\ t^2\ d^2$ I : $t^2$(?) z ŋ A
2. $b^2\ t^2$(?) $g^2$(?) $l^2$(?) $g^2$(?) $k^1$(?) $y^1$ A :/$s^2$(?) $b^2\ n^2\ t^2$(?) $d^2$ m : U/$k^2$ z $l^2\ g^2\ b^2\ k^2\ n^2$ m
3. $r^2$(?) $r^2$ ŋ č $b^2\ t^2\ d^2$ m
4. $t^2\ b^2$/ŋ $r^2\ n^2$

Its interpretation is then:

1. He has killed (lit.: reached) many (lit.: rich) wild animals // He has reached Beying // He has reached the home place (side). Hurry up (you all)!
2. A rock with inscription(s)! : I have written. // I have rejoiced. It is the best day in autumn for me (lit.: it is my autumn day)!
3. (Being) a hunter, I wrote.

Tengrin // With (the grace of) the heaven // God.

## 5. CONCLUSION

In the result of the performed tests, a method of the 3D digitization of the entire rock surfaces with submillimetric resolution was developed. The method is based on the SfM technology with the use of extension rings for the photography work ensuring the exact displacement of the camera, and with the incorporation of additional general view frames into the data processing for correcting the global deformation. The performed laboratory and field tests have shown that the developed method ensures building of 3D models of the surfaces with resolution up to 7.5 μm, minimal local accuracy 0.05 mm and maximal global deformation 1.2 mm (for the 920 mm long documented object). The used equipment is quite lightweight and mobile; it can be recommended for use in hard-to-reach places. In addition, the equipment and software are inexpensive and suit the ends of their non-commercial use. A drawback of the developed method of 3D documentation is a huge time consumption for the photography work (from 15 hours per one square meter). The method developed may also be used for documenting any planar objects requiring submillimetric resolution.

Manual tracings of the inscriptions on the basis of the built 3D models are far outnumbering the conventional tracing methods, although require more labor input and time consumption both for the field and office work. Thanks to advanced documentation technologies and the developed method, it has become possible to refine the tracing to a significant degree and propose readings of the D'odro I and Karban IV inscriptions, published here for the first time.

## ACKNOWLEDGEMENTS

This work was written in the framework of the project "Language and ethnocultural variability of Southern Siberia in synchrony and diachrony: language and culture interaction" (the RF Government grant No. 14.Y26.31.0014).

## REFERENCES

Agisoft. (2017). Script 'Split_in_chunks' for Agisoft Photoscan. Retrieved 14.02.2019, from http://wiki.agisoft.com/wiki/Split_in_chunks.py

Agisoft. (2018). Agisoft PhotoScan User Manual: Professional Edition. Copyright © 2018 Agisoft LLC.

Alexander, C., Pinz, A. and Reinbacher, C. (2015). Multi-scale 3D rock-art recording. *Digital Applications in Archaeology and Cultural Heritage*, Vol. 2, pp. 181–195.

Alimov, R., Kayrat, Tabaldiev, K. and Belek, K. (2010). A Newly Discovered Turkic Inscription in the Tian Shan Region: The Chiyin Tash Rock Inscription. *Altai Hakpo*, Vol. 20, pp. 187–195.

Artec. (2019). Space Spider Specifications. Retrieved 18 January 2019, from https://www.artec3d.com/files/pdf/Space-Spider-Booklet-EURO.pdf

Aydin, E., Alimov, R. and Yildirim, F. (2013). *Yenisey-Kırgızistan Yazıtları ve Irk Bitig*. Ankara, BilgeSu.

Bea, M. and Angás, J. (2017). Geometric documentation and virtual restoration of the rock art removed in Aragón (Spain). *Journal of Archaeological Science: Reports*, Vol. 11, pp. 159–168.

Cassen, S., Grimaud, V. and Lescop, L. (2015). Intuition and analysis in the recording, interpretation and public translation of Neolithic engraved signs in western France. *Digital Applications in Archaeology and Cultural Heritage,* Vol. 2, issues 2-3, pp. 213-221

Cassen, S., Lescop, L., Grimaud, V. and Robin, G. (2014). Complementarity of acquisition techniques for the documentation of Neolithic engravings: Lasergrammetric and photographic recording in Gavrinis passage tomb (Brittany, France). *Journal of Archaeological Science*, Vol. 45, pp. 126–140.

Clauson, sir G. (1966). Three notes on early Turkish. *Türk Dili Araştirmalari Yilligi-Belleten*, pp. 1–18.

Clini, P., Frapiccini, N., Mengoni, M., Nespeca, R. and Ruggeri, L. (2016). SFM technique and focus stacking for digital documentation of archaeological artifacts. *International Archives of the Photogrammetry, Remote Sensing and Spatial Information Sciences - ISPRS Archives*, Vol. XLI-B5, pp. 229–236.

Díaz-Guardamino, M., García Sanjuán, L., Wheatley, D. and Rodríguez Zamora, V. (2015). RTI and the study of engraved rock art: A re-examination of the Iberian south-western stelae of Setefilla and Almadén de la Plata 2 (Seville, Spain). *Digital Applications in Archaeology and Cultural Heritage*, Vol. 2, issues 2-3, pp. 41-54.

EDPT: Clauson sir G. (1972). An Etymological Dictionary of Pre-Thirteenth-Century Turkish. Oxford, at the Clarendon Press.

Elin, V. N., and Sojonov, V. I. (2013). Novye arxeologicheskie pamjatniki v zone planiruemogo stroitel'stva Katunskoj GES. *Arxeologicheskie issledovanija na Katuni*, Novosibirsk, Nauka, pp. 161–177.

Erdal, M. (1991). *Old Turkic Word Formation: A Functional Approach to the Lexicon* (Turcologica). Wiesbaden: Harrassowitz.

Erdal, M. (2002). Anmerkungen zu den Jenissei-Inschriften. *Splitter aus der Gegend von Turfan. Festschrift für Peter Zieme anläßlich seines 60, Geburtstags*, Istanbul–Berlin, Safak Matbaacilik, pp. 51-73.

Fernández-Lozano, J., Gutiérrez-Alonso, G., Ruiz-Tejada, M. Á., and Criado-Valdés, M. (2017). 3D digital documentation and image enhancement integration into schematic rock art analysis and preservation: The Castrocontrigo Neolithic rock art (NW Spain). *Journal of Cultural Heritage*, Vol. 26, pp. 160–166.

Gajski, D., Solter, A., and Gašparovic, M. (2016). Applications of macro photogrammetry in archaeology. *International Archives of the Photogrammetry, Remote Sensing and Spatial Information Sciences - ISPRS Archives*, Vol. XLI-B5, pp. 263–266.

Gallo, A., Muzzupappa, M., and Bruno, F. (2014). 3D reconstruction of small sized objects from a sequence of multi-focused images. *Journal of Cultural Heritage*, Vol. 15, pp. 173–182.

Georgopoulos, A., (2016) Photogrammetric automation: Is it worth? *Mediterranean Archaeology & Archaeometry*, vol.16, No.5, pp. 11-17.

Howland, M. D., Kuester, F., and Levy, T. E. (2014) Photogrammetry in the field:documenting, recording, and presenting archaeology. *Mediterranean Archaeology and Archaeometry*, Vol. 14, No 4, pp.101-108.

Jalandoni, A., Domingo, I., and Taçon, P. S. C. (2018). Testing the value of low-cost Structure-from-Motion (SfM) photogrammetry for metric and visual analysis of rock art. *Journal of Archaeological Science: Reports*, Vol. 17, pp. 605–616.

Kazakov, V., Kovalev, V. S., Zhumadilov, K., and S.V., S. (2016). Trekhmernaya vizualizatsiya geometricheskikh mikrolitov pri pomoshchi makrofotogrammetrii. *UNIVERSUM HUMANITARIUM*, Vol. 2, pp. 65–72.

Kindikov, B. M., and Kindikov, I. B. (2018). Drevnie pis'mena Ongudajskogo rajona. Gorno-Altaisk, Grono-Altajskaja tipografija.

Konkobaev, K., Useev, N., and Shabdanaliev, N. (2015). Atlas drevnetyurkskikh pis'mennykh pamyatnikov Respubliki Altay. Astana, International Turkic Academy.

Kontogianni, G., Chliverou, R., Koutsoudis, A., Pavlidis, G., and Georgopoulos, A. (2017). Enhancing close-up image based 3D digitisation with focus stacking. *International Archives of the Photogrammetry, Remote Sensing and Spatial Information Sciences - ISPRS Archives*, Vol. XLII-2/W5, pp. 421–425.

Kovalev, V. S., Volkov, P. V., Khaykunova, N. A., Lbova, L. V., and Bocharova, E. N. (2017). The Techniques of Modeling and Decorating Upper Paleolithic Anthropomorphic Figurines from Malta, Eastern Siberia. *Archaeology, Ethnology and Anthropology of Eurasia*, Vol. 45, Issue 3, pp. 48–55.

Kraus, K. (2007). Photogrammetry. Geometry from Images and Laser Scans. Berlin-New York, Walter de Gruyter.

Kyzlasov, I. L. (2002). *Pamjatniki runicheskoj pis'mennosti Gornogo Altaja*. Vol. 1, Gorno-Altajsk, Gorno-Altaisk State University.

Maté-González, M. Á., Aramendi, J., González-Aguilera, D., and Yravedra, J. (2017). Statistical comparison between low-cost methods for 3D characterization of cut-marks on bones. *Remote Sensing*, Vol. 9(873), pp. 1–17.

Maté González, M. Á., Yravedra, J., González-Aguilera, D., Palomeque-González, J. F., and Domínguez-Rodrigo, M. (2015). Micro-photogrammetric characterization of cut marks on bones. *Journal of Archaeological Science*, Vol. 62, pp. 128–142.

Matochkin, E. (1990). Graffiti Karbana. *Arxeologicheskie issledovanija na Katuni*, pp. 150–160.

Maue, D. (2018). Signs and Sounds. *Journal Asiatique*, Vol. 306, issue 2, pp. 291-301.

Mudge, M., Malzbender, T., Schroer, C., and Lum, M. (2006). New Reflection Transformation Imaging Methods for Rock Art and Multiple-Viewpoint Display. *Proceedings of the 7th International Symposium on Virtual Reality Archaeology and Cultural Heritage VAST2006*, Retrieved 25.02.2019 from http://culturalheritageimaging.org/What_We_Do/ /Publications/vast2006/VAST2006_final.pdf

Mudge, M., Voutaz, J., Schroer, C., and Lum, M. (2005). Reflection transformation imaging and virtual representations of coins from the hospice of the grand St. Bernard. *Proceedings of the 6th International Symposium on Virtual Reality Archaeology and Cultural Heritage VAST2006* Retrieved 25.02.2019 from http://culturalheritageimaging.org/ /What_We_Do/Publications/vast2005/VAST2005_final.pdf

Nevskaya, I. (2011). Some paleographic and orthographic features of Altay Runic inscriptions. Ülkü Čelik Šavk (Ed.), *Orkhon Yazïtlarïn Bulunušundan 120 Yïl sonra. Proceedings of the 3rd Runic symposium. Eski Türk yazıtları*. Ankara, Hacettepe University, pp. 589–599.

Nevskaya, I. (2015). Some orthographic features of Altai runic inscriptions. I. Nevskaya and M. Erdal (Eds.), *Interpreting Runic sources and the position of the Altay corpus.* (*Studien zur Sprache, Geschichte und Kultur der Türkvölker. Vol. 21)*. Berlin, Klaus Schwarz Verlag, Vol. 21, pp. 103–212.

Nevskaya, I. (2016). An Old Turkic Inscription Found in the Vicinity of the Village Jabogan of the Republic Altai: Its Paleographic Analysis and Reading. *BELLETEN Türk Dili Araştırmaları Yıllığı (BELLETEN Yearbook of Turkic Studies)*, Vol. 60, issue 1, pp. 39–57.

Nevskaya, I., and Tazhibayeva, S. (2019). Superlative readings of possessive constructions in Turkic. A comparative perspective. L. Johanson, L. Federica Mazzitelli, and I. Nevskaya (Eds.), *Possession and Ownership in the Languages of Europe and North and Central Asia. (Studies in Languages Companion Series. Vol. 206)*, Amsterdam, John Benjamins Publishing Company, pp. 205–238.

Nevskaya, I., Tybykova, L., Vavulin, M., Zaitceva, O., and Vodyasov, E. (2018). 3D documentation of Old Turkic Altai runiform inscriptions and revised readings of the inscriptions Tuekta-V and Bichiktu-Boom-III. *Turkic Languages*, Vol. 22, Issue 2, pp. 194–216.

Niederheiser, R., Mokros, M., Lange, J., Petschko, H., Prasicek, G.,Elberink, S. O. Deriving 3D point clouds from terrestrial photographs - Comparison of different sensors and software. (2016). *International Archives of the Photogrammetry, Remote Sensing and Spatial Information Sciences - ISPRS Archives*, Vol. XLI-B5, pp. 685–692.

Percoco, G., Lavecchia, F., and Salmerón, A. J. S. (2015). Preliminary study on the 3D digitization of millimeter scale products by means of photogrammetry. *Procedia CIRP*, Vol. 33, pp. 257–262.

Plisson, H. (2015). Digital photography and traceology: from 2d to 3d. *Traces in the History. Dedicated to 75 Anniversary of Viacheslav E. Shchelinsky*, pp. 216–231.

Plisson, H., and Zotkina, L. V. (2015). From 2D to 3D at macro- and microscopic scale in rock art studies. *Digital Applications in Archaeology and Cultural Heritage*, Vol. 2, issues 2-3, pp. 102–119.

Porter, S. T., Huber, N., Hoyer, C., and Floss, H. (2016). Portable and low-cost solutions to the imaging of Paleolithic art objects: A comparison of photogrammetry and reflectance transformation imaging. *Journal of Archaeological Science: Reports*, Vol. 10, pp. 859–863.

Robert, E., Petrognani, S., and Lesvignes, E. (2016). Applications of digital photography in the study of Paleolithic cave art. *Journal of Archaeological Science: Reports*, Vol. 10, pp. 847–858.

Rogerio-Candelera, M. Á. (2015). Digital image analysis based study, recording, and protection of painted rock art. Some Iberian experiences. *Digital Applications in Archaeology and Cultural Heritage*, Vol. 2, issues 2-3, pp. 68–78.

Şirin User, H. (2013). Yabogan (A 80) Yazıtı Üzerine. Bülent Gül (Ed.), *Bengü Beläk, Ahmet Bican Ercilasun Armağanı*, pp. 457-464.

Subbarao, M., and Choi, T. (1995). Accurate Recovery of Three-Dimensional Shape from Image Focus. *IEEE Transactions on Pattern Analysis and Machine Intelligence*, Vol. 17, pp. 266–274.

Tsiafaki, D and Michailidou, N (2015) Benefits and problems through the application of 3d technologies in archaeology: recording, visualisation, representation and reconstruction. *Scientific Culture*, Vol. 1, No 3, pp. 37-45.

Tybykova, L., Nevskaya, I., and Erdal, M. (2012). *Katalog drevnetjurkskix runičeskix pamjatnikov Gornogo Altaja.* Gorno-Altaysk, Gorno-Altajskoe knižnoe izdatel'stvo.

VATEC. *Vorislamische Alttürkische Texte: Elektronisches Corpus*. Retrieved 15.03.2019, from vatec2.fkidg1.uni-frankfurt.de.

Vavulin, M., Zaitceva, O., Nevskaya, I., Vodyasov, E., and Tybykova, L. (2018). Dokumentirovaniye drevnetyurkskikh runicheskikh naskal'nykh nadpisey Gornogo Altaya na osnove tekhnologii fotogrammetrii. *Virtual Archaeology (from Air, on Earth, under Water, at Museum)*, pp. 29–37.

Vavulin, M. V. (2017). Documentation of Old Turkic runic inscriptions of the Altai mountains using photogrammetric technology. *International Archives of the Photogrammetry, Remote Sensing and Spatial Information Sciences - ISPRS Archives*, Vol. XLII-2/W8, pp. 257–261.

Vavulin, M. V, Zaytseva, O. V, and Pushkaryov, A. A. (2014). 3D scanning techniques and practices used for different types of archaeological artifacts. *Siberian Historical Research*, issue 4, pp. 21–37.

Vovin, A. (2018). An Interpretation of the Hüis Tolgoi Inscription. *Journal Asiatique*, Vol. 306, issue 2, pp. 303-313.

Zeppelzauer, M., Poier, G., Seidl, M., Reinbacher, C., Schulter, S., Breiteneder, C. and Bischof, H. (2016). Interactive 3D Segmentation of Rock-Art by Enhanced Depth Maps and Gradient Preserving Regularization. *Journal on Computing and Cultural Heritage (JOCCH)* 9 (4):19